ORIGINAL ARTICLE

CrossMark

Comparative Cardiac Phantom Study Using Tc-99m/I-123 and Tl-201/I-123 Tracers with Cadmium-Zinc-Telluride Detector-Based Single-Photon Emission Computed Tomography

Takanaga Niimi[1] · Mamoru Nanasato[2] · Mitsuo Sugimoto[1] · Hisatoshi Maeda[3]

Abstract

Objective A recently introduced single-photon emission computed tomography (SPECT), based on cadmium-zinc-telluride (CZT) detectors (D-SPECT), supports high energy resolution for cardiac imaging. Importantly, the high energy resolution may allow simultaneous dual-isotope (SDI) imaging (e.g., using Tc-99m and I-123). We quantitatively evaluated Tc-99m/I-123 SDI imaging by D-SPECT in comparison with conventional T1-201/I-123.

Materials and Methods Energy resolution was measured as a percentage of the full width at half maximum (FWHM) for Tc-99m, I-123, and Tl-201. The impact of cross-talk and reconstructed image contrast were quantified by measuring the contrast-to-noise ratio (CNR), and the transmural defect contrast in the left ventricle wall (C_{TD}) induced by a difference in energy, for combinations of Tc-99m/I-123 or Tl-201/I-123, using an RH-2 cardiac phantom. Corresponding measurement was also carried out in Anger SPECT (A-SPECT).

Results The energy resolution of the D-SPECT system was 5.4%/5.1% for Tc-99m/I-123 and 5.4%/5.3% for Tl-201/I-123, which was approximately two times higher than the A-SPECT. No notable difference was confirmed in the CNRs of the two systems, but T1-201/I-123 showed overall higher value than Tc-99m/I-123. Compared to A-SPECT, C_{TD} of D-SPECT significantly increased with both Tc-99m/I-123 and T1-201/I-123 ($p < 0.05$). In DSPECT, the combination of Tc-99m/I-123 had a slightly better C_{TD} than T1-201/I-123. In addition, C_{TD} of Tc-99m/I-123 was improved with scatter correction at both nuclides ($p < 0.05$), but in Tl-201/I-123, no significant improvement was confirmed in I-123 ($p > 0.05$).

Conclusion D-SPECT was considered to be capable of performing high-quality SDI imaging using Tc-99m/I-123.

Keywords CZT detector · Energy resolution · Simultaneous dual-isotope SPECT · Cardiac imaging

Introduction

High sensitivity and high energy resolution single-photon emission computed tomography (SPECT), based on semiconductor detectors, presents unique possibilities for nuclear cardiac imaging [1–3]. Importantly, the high energy resolution provides a new opportunity for simultaneous dual-isotope (SDI) SPECT imaging using nuclide combinations such as Tc-99m and I-123 (Tc-99m/I-123) [4–7]. SDI-SPECT studies were first reported around 1978 [8], although few studies of combinations of new nuclides appeared until the cadmium-zinc-telluride (CZT) detector was developed recently. However, SDI-SPECT offers many advantages, such as examinations under the same physiological conditions, reduction of acquisition times, and improvements in patient throughput [9]. In the Anger SPECT (A-SPECT) system, we used a combination of Tl-201 and I-123 (Tl-201/I-123) to diagnose vaso-spastic angina in patients with acute myocardial infarction [10, 11]. We were hesitant to conduct that investigation because the combination requires a high dose of Tl-201, but recent remarkable improvements in D-SPECT indicate that it may now be feasible to carry out Tc-99m/I-123 SDI imaging

✉ Takanaga Niimi
nim@nagoya2.jrc.or.jp

1 Department of Radiological Technology, Nagoya Daini Red Cross Hospital, 2-9 Myouken-cho, Showa-ku, Nagoya 466-8650, Japan

2 Cardiovascular Center, Nagoya Daini Red Cross Hospital, 2-9 Myouken-cho, Showa-ku, Nagoya 466-8650, Japan

3 Department of Radiological Technology, Nagoya University School of Health Sciences, 1-1-20 Daiko-minami, Higashi-ku, Nagoya 461-8673, Japan

instead [12, 13], which involves lower doses of radiation but is difficult to perform with conventional A-SPECT. In this study, we quantitatively assessed Tc-99m/I-123 SDI imaging with D-SPECT.

Materials and Methods

Semiconductor-Based SPECT System

Our D-SPECT system (Spectrum Dynamics, Israel) is equipped with nine arrays of CZT detectors, with each detector block consisting of 16×64 individual pixels with a spacing of 2.46 mm in each dimension, resulting in a total detector surface of 39.4 mm $\times$ 157.6 mm [14–16]. Each detector can be rotated a maximum of 110° without moving parts and is equipped with a square tungsten parallel-hole collimator (septal thickness, 0.2 mm; pitch, 2.46 mm; and length, 21.7 mm) [14, 17]. Data acquisition was completed in approximately 10 min in all cases. Tc-99m/I-123 data were simultaneously acquired in energy windows centered at 140 keV (window width, 133–145 keV) for Tc-99m, and 159 keV (window width, 152–168 keV) for I-123 emission. Similarly, Tl-201/I-123 data were acquired at 70 keV (window width, 64–77 keV) for Tl-201, and 159 keV (window width, 152–168 keV) for I-123. The collected data were reformatted (matrix size, 64×64; voxel size, $4.92 \times 4.92 \times 4.92$ mm³) by reconstruction with and without scatter correction and reorientation. The scatter correction was processed using a scatter

correction method, designed for D-SPECT by Kacperski et al. [18].
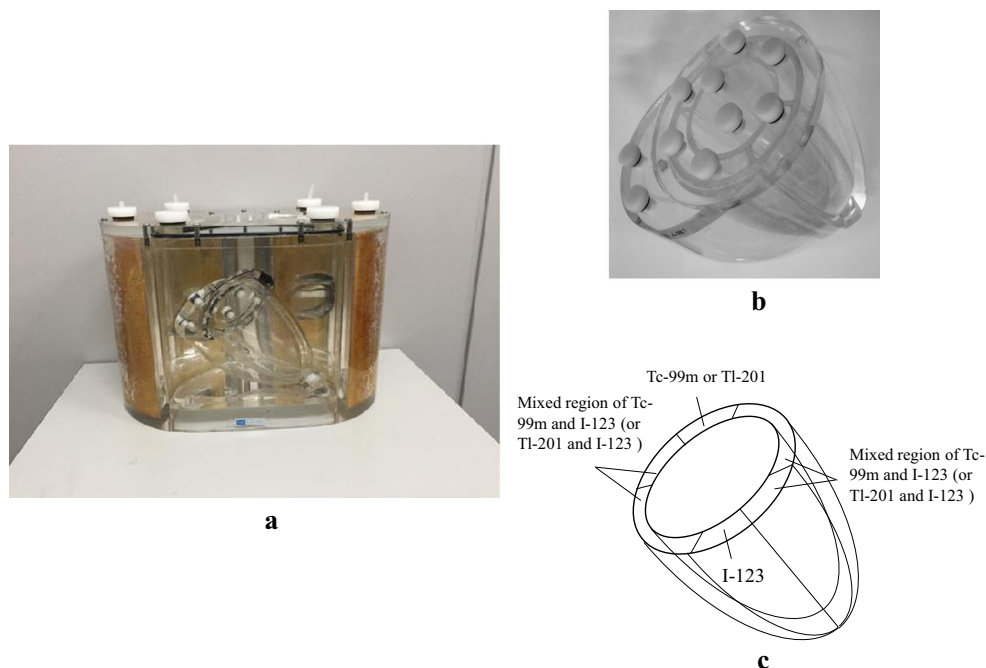
NaI-Based SPECT System

The NaI-based A-SPECT system (Bright-View; Philips, Japan) used for comparison with D-SPECT consisted of dual-head rotating detectors, and was equipped with a general-purpose low-energy collimator (septal thickness, 0.2 mm; pitch, 1.40 mm; length, 24.7 mm). A set of 32 projection images was obtained (step-and-shoot method, 25 s/ projection, 64×64 matrices) over a 90° arc. Energy peaks were set to Tc-99m (140 keV), I-123 (159 keV), and Tl-201 (70 keV) and energy window widths were set to 20%. The energy resolution (as a percentage of the full width at half maximum (FWHM)), measured in accordance with the National Electrical Manufacturers Association (NEMA) standard, is Tc-99m (9.9%), I-123 (10.1%), and Tl-201 (13.4%) [19]. Data acquisition was completed in approximately 15 min in all cases. The collected data were reformatted (matrix size, 64×64; voxel size, $6.39 \times 6.39 \times 6.39$ mm³) by reconstruction with a filtered back projection and reorientation. Scatter correction could not be used with A-SPECT.

Evaluation of the Energy Resolution

In D-SPECT, energy resolution was measured for Tc-99m (4.34 MBq/ml), I-123 (4.34 MBq/ml), and Tl-201 (4.34 MBq/ml) using tube phantoms (inner diameter, 9.5 mm; height, 300 mm; volume, 21.3 ml). Each nuclide

Fig. 1 **a** Structure of the RH-2 phantom. The phantom was made of acrylic and packed with an acrylic heart, Teflon spine, and wooden lungs. The mediastinal area was filled with water, and the size of the container simulated the human body. **b** Simulated cardiac phantom included in the RH-2 phantom. **c** Outline of the left ventricle of the cardiac phantom divided into six regions

was mixed in a tube phantom using a combination of Tc-99m/I-123 or Tl-201/I-123, and the percentage of FWHM, an index of energy resolution, was measured. In addition, we evaluated the energy resolution of the D-SPECT and A-SPECT systems for a combination of Tc-99m/I-123 or Tl-201/I-123 using an RH-2 phantom (Kyoto-Kagaku, Japan) (Fig. 1a). In the RH-2 phantom, the simulated cardiac phantom (Fig. 1b) was filled with water and fixed. The left ventricle (LV) in the cardiac phantom was divided into six regions (Fig. 1c), each filled with a solution of Tc-99m (0.25 MBq/ml) alone, a solution of I-123 (0.13 MBq/ml) alone, a mixture of Tc-99m (0.50 MBq/ml) and I-123 (0.26 MBq/ml), a solution of Tl-201 (0.19 MBq/ml) alone, a solution of I-123 (0.19 MBq/ml) alone, or a mixture of Tl-201 (0.38 MBq/ml) and I-123 (0.38 MBq/ml). The accuracy of the energy resolution in the system and reconstructed image contrast were evaluated in terms of a simulated transmural defect induced by a difference in energy. In addition, D-SPECT without detector rotation can cause image degradation on the inferior wall due to energy attenuation, as in the case of 180° collection of A-SPECT [20]. To verify this, we also evaluated the case where the cardiac phantom was rotated 180° as shown in Fig. 2a, and the position of the transmural defect was replaced from the anterior wall to the inferior wall (or vice versa).

Quantification of SDI Imaging

The accuracy of energy resolution and the impact of cross-talk were quantified by measuring the contrast-to-noise ratio (CNR) and the transmural defect contrast in the LV wall (C_{TD}) from the count values of a ventricular short-axis image. Region of interest (ROI) dimensions and locations of the myocardium and the transmural defect, used for quantitative analysis, were set using the Image J software. By rotating the cardiac phantom 180°, the ROI was set in a simulated transmural defect on the anterior wall side and the inferior wall side for each nuclide (Fig. 2b). The area of the background region used for the measurement of the CNR was set to be almost the same as the area of the myocardial region. The same ROI was set for the 10-slice ventricular short-axis image simultaneously obtained from one phantom experiment, and the average and standard deviation of CNR and C_{TD} obtained from each image were calculated. CNR and C_{TD} were calculated using the following equations [21]:

$$CNR = (M_{my} - M_{BG}) / \sqrt{SD_{my}^2 - SD_{BG}^2}, \qquad (1)$$

where M_{my} is mean myocardial counts, M_{BG} is mean background counts, SD_{my} is mean myocardial standard deviation (SD), and SD_{BG} is mean background SD.
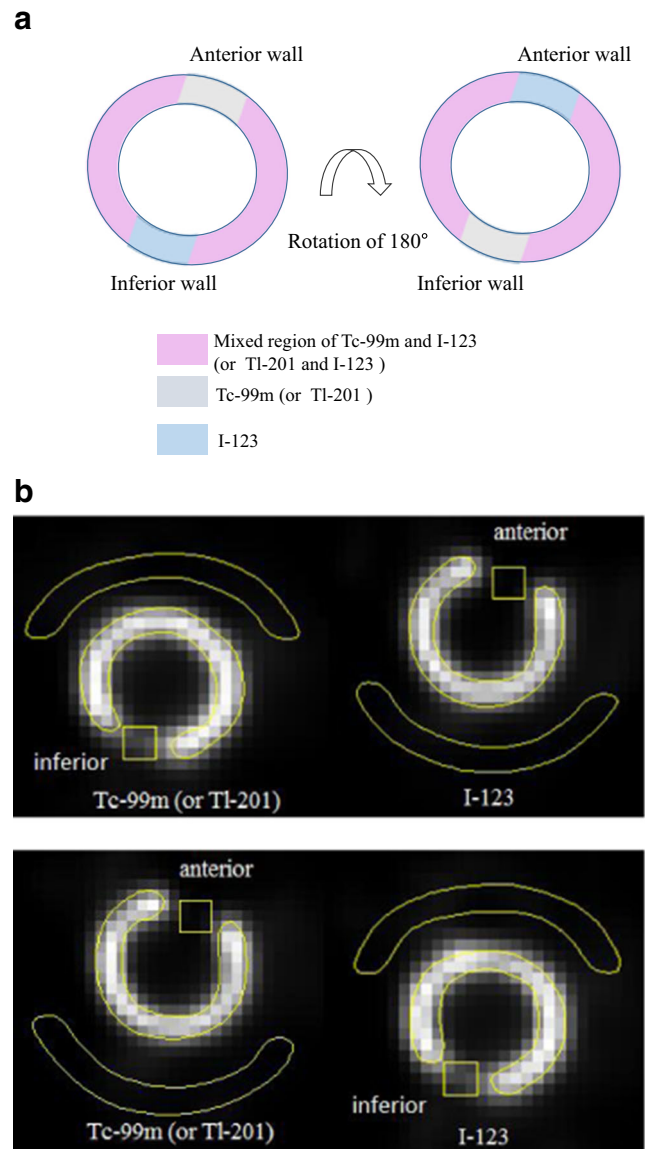

Fig. 2 **a** Outline of the image obtained by slicing the cardiac phantom in the short-axis direction. Right panel depicts the image where the cardiac phantom is rotated 180°. **b** Region of interest dimensions and location used for quantitative analysis, created using the Image J software for a combination of Tc-99m/I-123 or Tl-201/I-123. Lower panel depicts the image where the cardiac phantom is rotated 180°

C_{TD} was defined as the percentage difference between M_{my} and M_{TD}:

$$C_{TD} (\%) = \left[(M_{my} - M_{TD}) / M_{my} \right] \times 100 \qquad (2)$$

where M_{my} is the mean myocardial count and M_{TD} is the transmural defect count. The ideal value for C_{TD} is 100%.

To clarify the correlation between quantitative evaluation and visual evaluation, two cardiologists (experience, 5 and 26 years) and two radiological technologists (clinical experience, 26 and 33 years) participated in a phantom observation test, in which they compared images subjectively in qualitative terms [4].

Results

Figure 3 shows the energy spectrum of the D-SPECT and A-SPECT systems for (a) Tc-99m/I-123 and (b) Tl-201/I-123. The energy resolution (percentage of FWHM) of the D-SPECT system obtained from the data shown in the figures was 5.4%/5.1% for Tc-99m/I-123 and 5.4%/5.3% for Tl-201/I-123, which was approximately two times higher than that of A-SPECT. Figure 4 shows the comparison of the D-SPECT and A-SPECT systems on the short axis images without scatter correction, for Tc-99m/I-123 or Tl-201/I-123. Table 1 shows the CNR and C_{TD} calculated from the data shown in

Fig. 3 The energy spectrum of the D-SPECT and A-SPECT systems at **a** Tc-99m/I-123 and **b** Tl-201/I-123. The dotted line shows the energy window width of D-SPECT
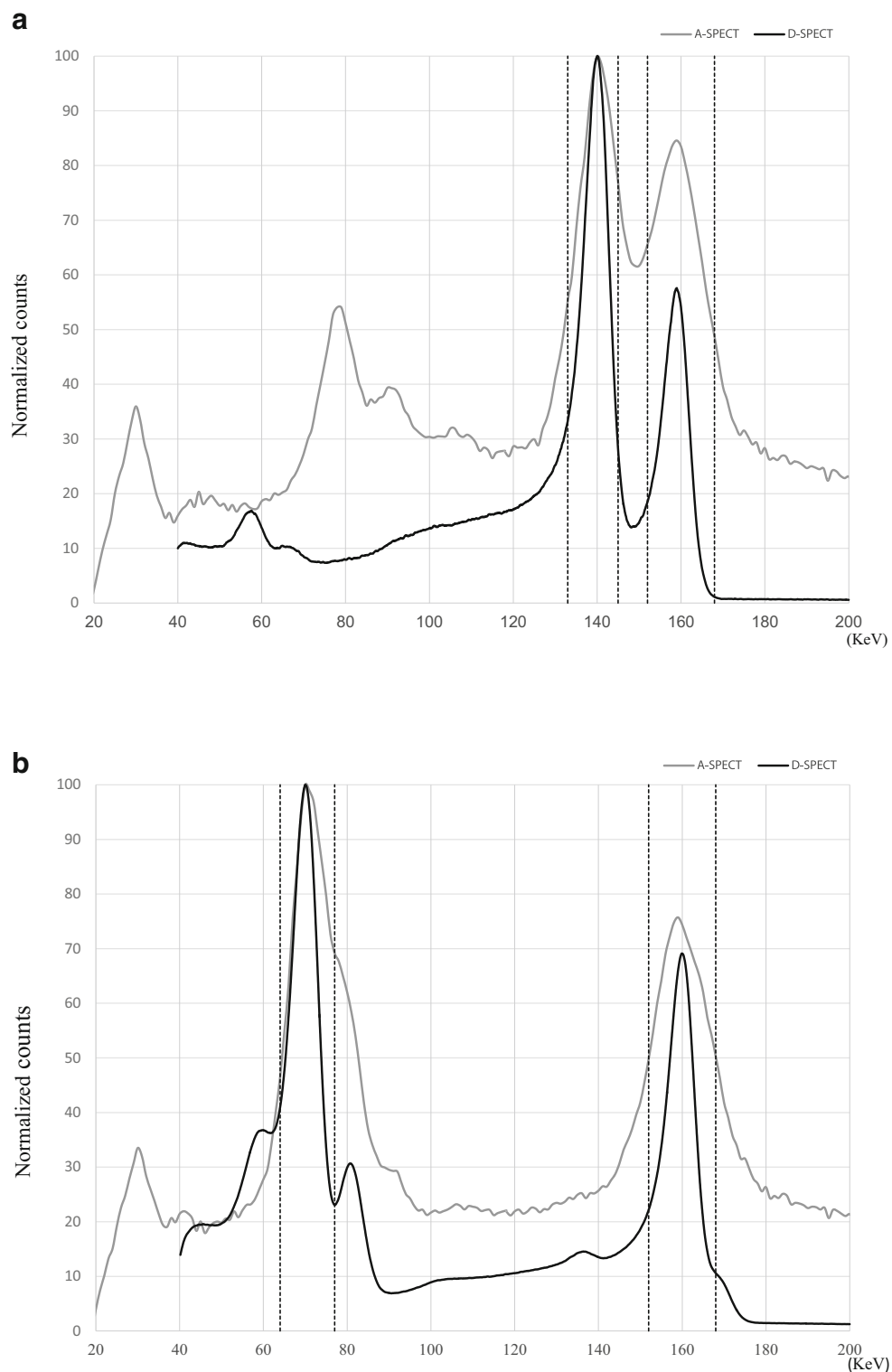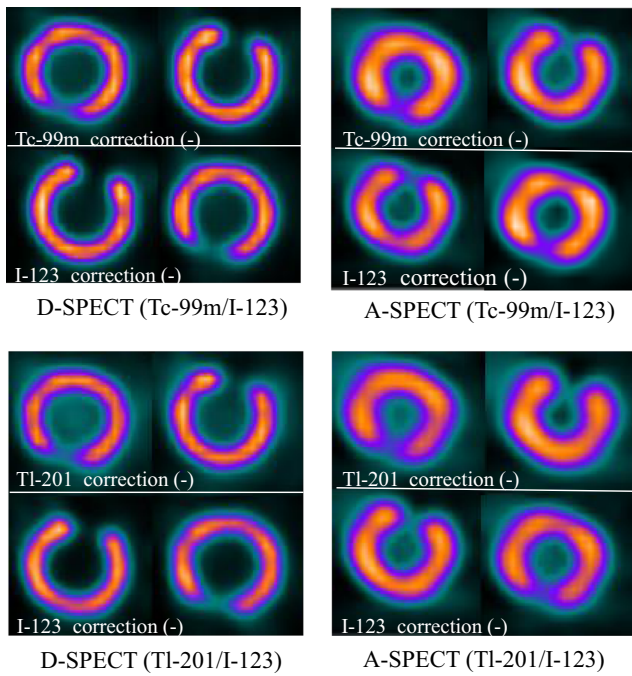
Fig. 4 Comparison of the D-SPECT and A-SPECT systems on the cardiac phantom images (short axis slices) without scatter correction, for Tc-99m/I-123 or Tl-201/I-123

those figures. No notable difference was confirmed in the CNRs of the two systems; however, the combination of Tc-99m/I-123 in D-SPECT increased C_{TD} by 28.7% for Tc-99m and 51.4% for I-123 in the anterior wall compared to A-SPECT without scatter correction. Similarly, the combination of Tl-201/I-123 increased 21.3% for Tl-201 and 21.4% for

Table 1 Comparison of the image quality of D-SPECT and A-SPECT images without scatter correction

	Combination	Isotope	Position of defect	CNR mean (SD)	C_{TD} (%) mean (SD)
A-SPECT	Tc-99m/I-123	Tc-99m	Anterior	4.5 (0.2)	61.9 (2.8)
			Inferior	4.5 (0.2)	37.4 (1.6)
		I-123	Anterior	4.4 (0.3)	43.5 (3.8)
			Inferior	4.2 (0.5)	25,6 (1.4)
	Tl-201/I-123	Tl-201	Anterior	4.5 (0.2)	65.1 (2.0)
			Inferior	5.2 (0.3)	43.1 (2.2)
		I-123	Anterior	5.0 (0.3)	68.6 (1.4)
			inferior	5.1 (0.2)	36.6 (2.5)
D-SPECT	Tc-99m/I-123	Tc-99m	Anterior	4.1 (0.2)	90.6 (1.3)
			Inferior	4.2 (0.2)	70.3 (1.0)
		I-123	Anterior	4.5 (0.2)	94.9 (1.2)
			Inferior	4.4 (0.3)	64.3 (2.5)
	Tl-201/I-123	Tl-201	Anterior	4.7 (0.2)	86.4 (2.0)
			Inferior	4.5 (0.1)	71.7 (2.8)
		I-123	Anterior	4.7 (0.2)	90.0 (2.0)
			Inferior	4.7 (0.2)	75.5 (3.3)

I-123. Regarding the inferior wall, C_{TD} was 15 to 30% lower than that of the anterior wall in both systems, although a similar improvement was confirmed. In DSPECT, the combination of Tc-99m/I-123 had a slightly better C_{TD} than T1-201/I-123.

Figure 5 shows short axis images of D-SPECT for (a) Tc-99m/I-123 and (b) Tl-201/I-123, with and without scatter correction, and Table 2 shows the CNR and C_{TD} calculated from the
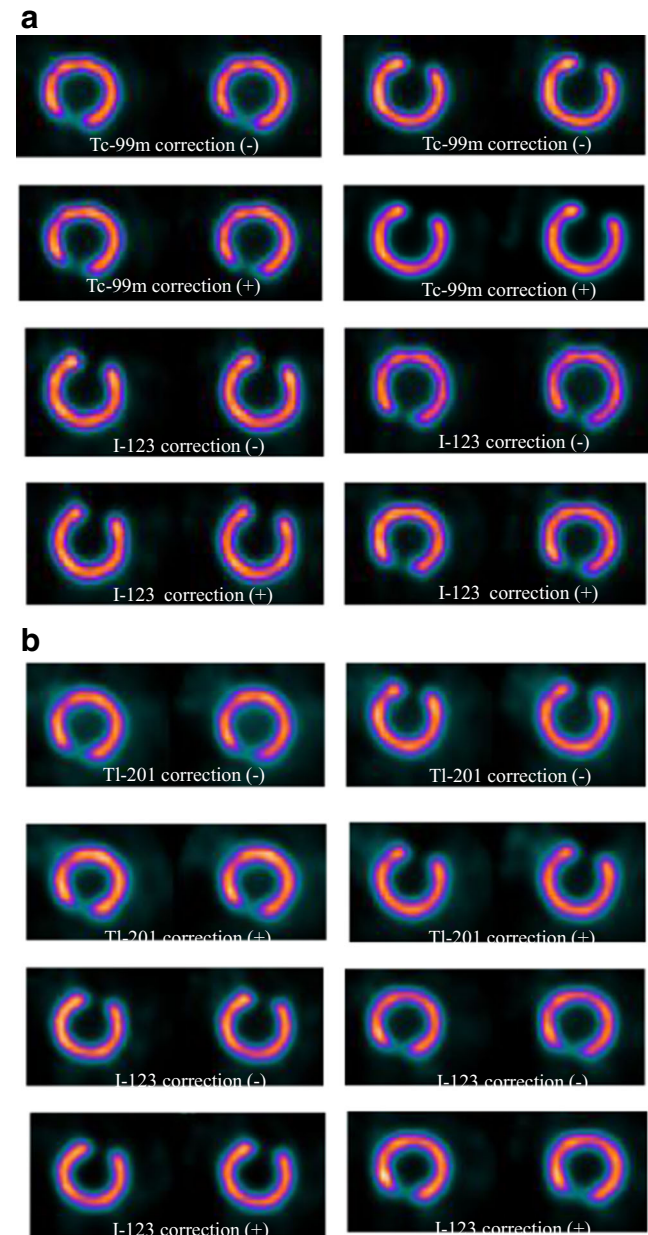

Fig. 5 Short-axis images from the D-SPECT system of the cardiac phantom, with and without scatter correction, for **a** Tc-99m/I-123 and **b** Tl-201/I-123. Right panels depict the case where the cardiac phantom is rotated 180° for each nuclide. In a combination of Tc-99m/I-123, the scattering correction reduced the collection counts by approximately 31% for Tc-99m and by approximately 24% for I-123. Similarly, the combination of Tl-201/I-123 showed counts reduced by approximately 53% for Tl-201 and by approximately 27% for I-123

Table 2 Image quality of Tc-99m/I-123 and Tl-201/I-123 SDI imaging for D-SPECT with and without scatter correction

Combination	Isotope	Correction	Position of defect	CNR mean (SD)	C_{TD} (%) mean (SD)
Tc-99m/I-123	Tc-99m	–	Anterior	4.1 (0.2)	90.6 (1.3)
			Inferior	4.2 (0.2)	70.3 (1.0)
	I-123	–	Anterior	4.5 (0.2)	94.9 (1.2)
			Inferior	4.4 (0.3)	64.3 (2.5)
	Tc-99m	+	Anterior	4.2 (0.2)	97.3 (1.8)
			Inferior	4.5 (0.2)	80.3 (2.3)
	I-123	+	Anterior	4.8 (0.3)	98.1 (1.6)
			Inferior	4.5 (0.2)	68.3 (3.5)
Tl-201/I-123	Tl-201	–	Anterior	4.7 (0.2)	86.4 (2.0)
			Inferior	4.5 (0.1)	71.7 (2.8)
	I-123	–	Anterior	4.7 (0.2)	90.0 (2.0)
			Inferior	4.7 (0.2)	75.5 (3.3)
	Tl-201	+	Anterior	4.6 (0.2)	92.6 (2.2)
			Inferior	4.8 (0.1)	82.8 (3.7)
	I-123	+	Anterior	4.7 (0.2)	90.7 (2.5)
			Inferior	4.8 (0.2)	77.1 (3.9)

corresponding data. C_{TD} of Tc-99m/I-123 was improved with scatter correction at both nuclides ($p < 0.05$), but in Tl-201/I-123, no significant improvement was confirmed in I-123 ($p > 0.05$). In the inferior wall, CNR improved 0.3 in both nuclides, C_{TD} improved by 10% at Tc-99m and 11.1% at Tl-201.

Discussion

We carried out a phantom experiment to quantitatively assess the merits of Tc-99m/I-123 SDI imaging with D-SPECT. The semiconductor-based D-SPECT system provided approximately two times higher energy resolution than the conventional A-SPECT system for Tc-99m and I-123 [4, 19], implying better image quality and less cross-talk with the simultaneous use of dual isotopes. We carried out image reconstruction with and without scatter correction to examine the influence of cross-talk on SDI imaging [22]. The effects of cross-talk for Tc-99m/I-123 and Tl-201/I-123 SDI imaging could be detected by quantitative analysis such as CNR or C_{TD}, and visual inspection of the RH-2 phantom images. As shown in Table 2, when scatter correction was used, the image quality for Tc-99m and Tl-201 were both improved in comparison with the results when no scatter correction was applied ($p < 0.05$). D-SPECT without detector rotation also proved to cause image degradation of the inferior wall due to energy attenuation, as in the case of 180° collection of A-SPECT. As a countermeasure against this, scatter correction was considered to be one effective means. By using scatter correction, the image quality of the inferior wall, CNR improved by 0.3, C_{TD} by 10% at Tc-99m and 11.1% at Tl-201.

Therefore, it was considered effective to use scatter correction for Tc-99m and Tl-201 in the case of SDI imaging. In a combination of Tc-99m/I-123, the collection counts decreased by approximately 31% for Tc-99m and by approximately 24% for I-123. Similarly, the combination of Tl-201/I-123 showed counts reduced by approximately 53% for Tl-201 and by approximately 27% for I-123. When using scatter correction clinically, it seems necessary to set the collection time so that the LV count will be 1 M counts or more [23]. I-123 was poorer in system sensitivity than Tc-99m or Tl-201 [19], and the improvement in image quality produced by scatter correction was also small (less than 5%), so we conclude that it is better to prioritize count acquisition over scatter correction. Conventionally, we had used a combination of Tl-201-Cl (111 MBq)/I-123-15-odophenyl 3-methyl pentadecanoic acid (111 MBq) to diagnose vasospastic angina with A-SPECT [11]. However, Einstein et al. [12] have reported avoidance of the use of thallium as a dual-isotope cardiac tracer. Tc-99m/I-123 SDI imaging with D-SPECT has benefits such as reduction of the injection dose by changing the nuclide from Tl-201 to Tc-99m. D-SPECT was considered to be capable of performing high-quality SDI imaging using Tc-99m/I–123 as with Tl-201/I-123.

Conclusion

D-SPECT was considered to be capable of performing high-quality SDI imaging using Tc-99m/I-123, and further improvement of image quality can be expected by using scatter correction.

Compliance with Ethical Standards

Conflict of Interest Takanaga Niimi, Mamoru Nanasato, Mitsuo Sugimoto, and Hisatoshi Maeda declare that they have no conflict of interest.

Ethical Approval This study was approved by the institutional review board of the hospital on October 25, 2016 and has been performed in accordance with the ethical standards laid down in the Helsinki Declaration of 1964 and later revision.

Informed Consent All subjects in the study gave written informed consent or the institutional review board waived the need to obtain informed consent.

Publisher's Note Springer Nature remains neutral with regard to jurisdictional claims in published maps and institutional affiliations.

References

1. Garcia EV, Faber TL, Esteves FP. Cardiac dedicated ultrafast SPECT cameras: new designs and clinical implications. J Nucl Med. 2011;52:210–7.
2. Neill J, Prvulovich EM, Fish MB, Berman DS, Slomka PJ, Sharir T, et al. Initial multicenter experience of high-speed myocardial perfusion imaging: comparison between high-speed and conventional single-photon emission computed tomography with angiographic validation. Eur J Nucl Med Mol Imaging. 2013;40:1084–94.
3. Duvall WL, Slomka PJ, Gerlach JR, Sweeny JM, Baber U, Croft LB, et al. High-efficiency SPECT MPI: comparison of automated quantification, visual interpretation, and coronary angiography. J Nucl Cardiol. 2013;20:763–73.
4. Ben-Haim S, Kacperski K, Hain S, Van Gramberg D, Hutton BF, Erlandsson K, et al. Simultaneous dual-radionuclide myocardial perfusion imaging with a solid-state dedicated cardiac camera. Eur J Nucl Med Mol Imaging. 2010;37:1710–21.
5. Ko T, Utanohara Y, Suzuki Y, Kurihara M, Iguchi N, Umemura J, et al. A preliminary feasibility study of simultaneous dual-isotope imaging with a solid-state dedicated cardiac camera for evaluating myocardial perfusion and fatty acid metabolism. Heart Vessel. 2016;31:38–45.
6. Kobayashi M, Matsunari I, Nishi K, Mizutani A, Miyazaki Y, Ogai K, et al. Simultaneous acquisition of (99m)Tc- and (123)I-labeled radiotracers using a preclinical SPECT scanner with CZT detectors. Ann Nucl Med. 2016;30:263–71.
7. Blaire T, Bailliez A, Bouallegue FB, Bellevre D, Agostini D, Manrique A. Left ventricular function assessment using ^{123}I/^{99m}Tc dual-isotope acquisition with two semi-conductor cadmium–zinc–telluride (CZT) cameras: a gated cardiac phantom study. EJNMMI Phys. 2016;3:27–37.
8. Berger HJ, Gottschalk A, Zaret BL. Dual radionuclide study of acute myocardial infarction: comparison of thallium-201 and technetium-99m stannous prophosphate imaging in man. Ann Intern Med. 1978;88:145–54.
9. Tsuji A, Kojima A, Matsumoto M, Oyama Y, Tomiguchi S, Kira T, et al. A new method for crosstalk correction in simultaneous dual-isotope myocardial imaging with Tl-201 and I-123. Ann Nucl Med. 1999;13:317–23.
10. Nakajima K, Shimizu K, Taki J, Uetani Y, Konishi S, Tonami N, et al. Utility of iodine-123-BMIPP in the diagnosis and follow-up of vasospastic angina. J NucI Med. 1995;36:1934–40.
11. Yamagishi H, Akioka K, Shirai N, Yoshiyama M, Teragaki M, Takeuchi K, et al. Effects of smoking on myocardial injury in patients with conservatively treated acute myocardial infarction—a study with resting 123I-15-iodophenyl 3-methyl pentadecanoic acid/201Tl myocardial single photon emission computed tomography. Jpn Circ J. 2001;65:769–74.
12. Einstein AJ, Moser KW, Thompson RC, Cerqueira MD, Henzlova MJ. Radiation dose to patients from cardiac diagnostic imaging. Circulation. 2007;116:1290–305.
13. Einstein AJ, Pascual TNB, Mercuri M, Karthikeyan G, Vitola JV, Mahmarian JJ, et al. Current worldwide nuclear cardiology practices and radiation exposure: results from the 65 country IAEA Nuclear Cardiology Protocols Cross-Sectional Study (INCAPS). Eur Heart J. 2015;36:1689–96.
14. Gambhir SS, Berman DS, Ziffer J, Nagler M, Sandler M, Patton J, et al. A novel high-sensitivity rapid-acquisition single-photon cardiac imaging camera. J Nucl Med. 2009;50:635–43.
15. Erlandsson K, Kacperski K, van Gramberg D, Hutton BF. Performance evaluation of D-SPECT: a novel SPECT system for nuclear cardiology. Phys Med Biol. 2009;54:2635–49.
16. Verger A, Imbert L, Yagdigul Y, Fay R, Djaballah W, Rouzet F, et al. Factors affecting the myocardial activity acquired during exercise SPECT with a high-sensitivity cardiac CZT camera as compared with conventional Anger camera. Eur J Nucl Med Mol Imaging. 2014;41:522–8.
17. Park MA, Moore SC, Muller SP, McQuaid SJ, Kijewski MF. Performance of a high-sensitivity dedicated cardiac SPECT scanner for striatal uptake quantification in the brain based on analysis of projection data. Med Phys. 2013;40:042504.
18. Kacperski K, Erlandsson K, Ben-Haim S, Hutton BF. Iterative deconvolution of simultaneous 99mTc and 201Tl projection data measured on a CdZnTe-based cardiac SPECT scanner. Phys Med Biol. 2011;56:1397–414.
19. Niimi T, Sugimoto M, Nanasato M, Maeda H. Evaluation of cadmium-zinc-telluride detector-based single-photon emission computed tomography for nuclear cardiology: a comparison with conventional Anger single-photon emission computed tomography. Nucl Med Mol Imaging. 2017;51:331–7.
20. Esquerre JP, Coca FJ, Martinez SJ, Guiraud RF. Prone decubitus: a solution to inferior wall attenuation in thallium-201 myocardial tomography. J Nucl Med. 1989;30:398–401.
21. Zoccarato O, Lizio D, Savi A, Indovina L, Scabbio C, Leva L, et al. Comparative analysis of cadmium-zincum-telluride cameras dedicated to myocardial perfusion SPECT: a phantom study. J Nucl Cardiol. 2016;23:885–93.
22. Kadrmas DJ, Frey EC, Tsui BMW. Simultaneous technetium-99*m*/thallium-201 SPECT imaging with model-based compensation for cross-contaminating effects. Phys Med Biol. 1999;44:1843–60.
23. Nakazato R, Berman DS, Hayes SW, Fish M, Padgett R, Xu Y, et al. Myocardial perfusion imaging with a solid-state camera: simulation of a very low dose imaging protocol. J Nucl Med. 2013;54:373–9.